Single-molecule orientation measurements with a quadrated pupil

Adam S. Backer,[1,2] Mikael P. Backlund,[2] Matthew D. Lew,[2,3] and W. E. Moerner[2,*]

[1]*Institute of Computational and Mathematical Engineering, 475 Via Ortega, Stanford, California 94305, USA*

[2]*Department of Chemistry, Stanford University, 375 North-South Axis, Stanford, California 94305, USA*

[3]*Department of Electrical Engineering, 350 Serra Mall, Stanford, California 94305, USA*

**Corresponding author: wmoerner@stanford.edu*

Received January 7, 2013; revised March 11, 2013; accepted March 13, 2013;
posted March 15, 2013 (Doc. ID 182888); published April 29, 2013

This Letter presents a means of measuring the dipole orientation of a fluorescent, orientationally fixed single molecule, which uses a specially designed phase mask, termed a "quadrated pupil," conjugate to the back focal plane of a conventional wide-field microscope. The method leverages the spatial anisotropy of the far-field emission pattern of a dipole emitter and makes this anisotropy amenable to quantitative analysis at the image plane. In comparison to older image-fitting techniques that infer orientation by matching simulations to defocused or excessively magnified images, the quadrated pupil approach is more robust to minor modeling discrepancies and optical aberrations. Precision of 1°–5° is achieved in proof-of-concept experiments for both azimuthal (φ) and polar (θ) angles without defocusing. Since the phase mask is implemented on a liquid-crystal spatial light modulator that may be deactivated without any mechanical perturbation of the sample or imaging system, the technique may be readily integrated into clear aperture imaging studies.

OCIS codes: (070.6110) Spatial filtering; (110.1758) Computational imaging; (110.4850) Optical transfer functions; (180.2520) Fluorescence microscopy.

http://dx.doi.org/10.1364/OL.38.001521

Single-molecule microscopy has long recognized the utility of measuring a fluorophore's dipole orientation [1]. A variety of methods have been employed ranging from the use of polarization optics [2–4] to precise recording of the distorted image which occurs upon defocusing a wide-field microscope [5,6]. Orientation studies have shed light on numerous biological processes [3,4,6,7]. Furthermore, orientation must be taken into account when attempting to ascertain the *positions* of single molecules (SMs) from microscope images, so as to avoid localization errors that result when using rudimentary fitting schemes [8,9]. Our approach infers polar inclination without total internal reflection fluorescence (TIRF) excitation, and only one polarizer is used in the emission pathway. Precise modeling of minor defocus aberration is not required. Furthermore, in-focus SMs may be analyzed, even if the effective detector pixel size is large. Given a fixed photon budget, the technique presented in this Letter trades position information for a higher-precision orientation measurement using a single camera frame.

Our technique uses an experimental setup identical to the one presented in [9], which adds Fourier plane processing to a conventional inverted epifluorescence microscope. Briefly, using a polarizing beam splitter, fluorescence exiting the microscope is separated into a reflected (R) and a transmitted (T) channel (respectively containing s- and p-polarized light, as defined relative to the surface of the beam splitter). Using a $4f$ optical processing configuration, the electric fields of the two polarizations are Fourier transformed and projected onto a spatial light modulator (SLM) programmed with the quadrated phase mask [Fig. 1(a)]. Modulated light from each polarization channel is Fourier transformed again, then relayed onto a separate region of an electron-multiplying charge-coupled device (EMCCD). The resulting SM emission patterns may be expressed as

$$E^{R}_{\mathrm{DET}}(x',y') = \mathrm{R}\{\mathrm{FT}\{e^{i\psi(\xi,\eta)}\mathrm{FT}\{E^{S}_{IP}(x,y)\}\}\}$$
$$E^{T}_{\mathrm{DET}}(x',y') = \mathrm{FT}\{e^{i\psi(\xi,\eta)}\mathrm{FT}\{E^{S}_{IP}(x,y)\}\}, \quad (1)$$

$E^{S,P}_{IP}(x,y)$ denote the s- or p-polarized portion of the electric field at the microscope's image plane (prior to optical processing), and $E^{R,T}_{\mathrm{DET}}(x',y')$ represent the resulting electric fields in the R and T channels at the detector. FT{} is the Fourier transform operation, and R{} denotes a reflection operation about the y' axis, which arises from

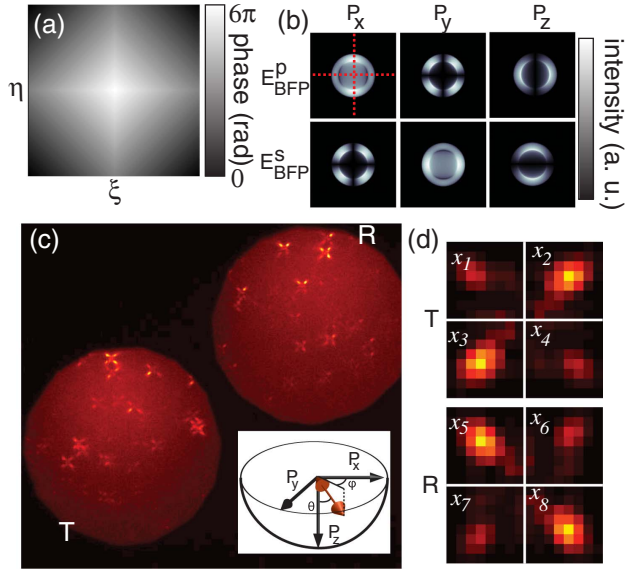

Fig. 1. (a) Quadrated phase mask. (b) Simulated emission patterns at the back focal plane. Dotted red lines indicate quadrant boundaries of phase mask. (c) Wide-field image of the R and T polarization channels. Inset: parameterization of dipole orientation P. (d) R and T images used to infer SM orientation (simulated).

the fact that the R channel incurs one additional reflection on account of the beam splitter. $\psi(\xi,\eta)$ is the phase modulation imparted by the SLM. When the phase mask is in use, this term may be expressed as the following pyramid-shaped aberration consisting of four linear phase ramps:

$$\psi(\xi,\eta) = C_0 - C(|\xi| + |\eta|). \tag{2}$$

The constant C_0 is set by the dynamic range of the SLM ($\sim 6\pi$), and $C = C_0/\rho_{\max}$, where $\rho_{\max}$, is the radius of the region in which intensity may be nonzero, as enforced by the numerical aperture, magnification, and the focal lengths of the lenses used in the $4f$ system.

A sample wide-field fluorescence image is presented in Fig. 1(c). Each molecule appears as a four-pointed star in each polarization channel. Hence, a total of eight "spots" are observed [Fig. 1(d)]. Intuitively, light emitted by a molecule falling upon a given quadrant is shunted into one of the eight spots recorded by the EMCCD. Vectorial optical calculations reveal that the far-field dipole emission pattern asymmetrically illuminates the phase mask as a function of orientation [10,11], and will cause these spots to have differing intensities. Since the quadrants of the phase mask align with the symmetries present in the polarized electric fields of dipoles oriented along the x, y, and z axes [Fig. 1(b)], we ensure high sensitivity throughout the range of all possible orientations a dipole may assume. To estimate orientation, a molecule of interest is identified in both the T and R channels, and the number of photons in each of the eight spots is calculated. Photon counts are stored in a vector x. The maximum-likelihood estimate of a given orientation is achieved by maximizing the (Poisson) objective function [12]:

$$O(\theta,\varphi) = \sum_{i=1}^{8} x_i \ln(y_i + Nb) - (y_i + Nb). \tag{3}$$

$O(\theta,\varphi)$ is related to the log-likelihood, $l(x,b|\theta,\varphi)$, by addition of a constant, which may be neglected since it does not influence the optimization procedure. b is the mean background fluorescence per pixel, and N is the number of pixels in the region used to calculate a given x_i. The eight-element expected image vector y is determined by simulating an intensity-scaled image of a dipole emitter fixed at orientation (θ,φ) embedded at an air–glass interface, and incorporating the quadrated phase mask using Eqs. (1) and (2). The resulting simulated images are then divided into eight subregions over which intensities are summed. Orientation measurements are interchangeably represented as a pair of angles, or as a point on the unit-hemisphere:

$$P = \{P_x, P_y, P_z\} = \{\sin(\theta)\cos(\varphi), \sin(\theta)\sin(\varphi), \cos(\theta)\}.$$

As a proof of concept, nanomolar concentrations of the fluorophore dicyanomethylenedihydrofuran-N-6 (DCDHF-N-6) in 1% polymethyl methacrylate (PMMA) were spin-coated onto microscope coverslips to form a film of orientation-fixed molecules ~50 nm thick [9]. Samples were imaged by an Olympus IX71 microscope with a 100 × /1.4 NA Olympus UPlanSApo oil immersion objective. Excitation was achieved with circularly polarized 514 nm light from an Ar-ion laser. ~0.1 kW/cm^2 peak intensity was measured at the sample. Fluorescence at 609 nm was filtered by a Chroma Z514RDC dichroic and a 590/60 bandpass filter. Optical processing was performed using a Boulder Nonlinear XY Phase Series SLM. Images were captured on an Andor iXon + EMCCD with a gain of 300 and an effective pixel size of 160 nm.

The quadrated phase mask was loaded onto the SLM, and twenty 1-s exposures were acquired. Orientation measurements were performed for the same molecule using separate images. Results for representative molecules Mol. 1 and Mol. 2 are shown in Fig. 2. Note that

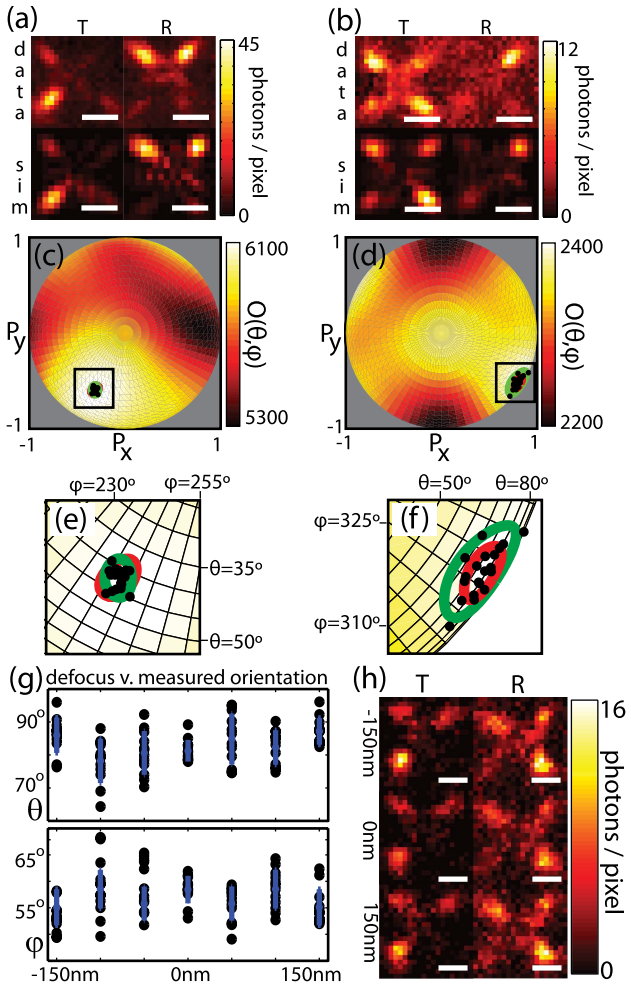

Fig. 2. Orientation measurements for two representative SMs. (a) and (b) (top row) Data collected for Mol. 1 and Mol. 2, respectively, and (bottom row) simulated images generated using orientation estimates inferred from this data (scale bar is 1 μm). (c) and (d) Plots of objective-function evaluations throughout the unit hemisphere. Overlaid on these plots are the results of repeated orientation measurements of the same molecule (black dots). The 2σ ellipse predicted by the CRLB and the data-covariance matrix are plotted in red and green, respectively. (e) and (f) Enlarged regions of interest in (c) and (d), respectively. Black lines represent 5° angular increments. (g) Orientation measurements as a function of depth (black dots) for the molecule Mol. 3. Standard deviations at each depth are denoted by blue lines. (h) Images of Mol. 3 with different amounts of defocus.

Table 1. Fitting Statistics for Representative Molecules

	Photons	$\sigma^{\theta}_{\mathrm{CRLB}}$	$\sigma^{\varphi}_{\mathrm{CRLB}}$	$\sigma^{\theta}_{\mathrm{data}}$	$\sigma^{\varphi}_{\mathrm{data}}$	$\theta_{\mathrm{avg.}}$	$\varphi_{\mathrm{avg.}}$
Mol. 1	2370	1.9°	1.5°	1.8°	1.7°	42.2°	242.2°
Mol. 2	921	3.4°	2.4°	5.8°	4.3°	73.9°	326.9°
Mol. 3	916	2.8°	2.0°	6.3°	4.3°	82.9°	57.0°
Mol. 1 (*600-nm clear aperture defocus*):				3.9°	3.2°	36.0°	260.7°
Mol. 2 (*600-nm clear aperture defocus*):				12.0°	2.8°	74.2°	347.1°

$O(\theta, \varphi)$ has few local maxima, facilitating the use of standard optimization procedures. To compute the ultimate limit of precision of our method, the Cramer–Rao lower bound (CRLB) was calculated [12], and 2σ ellipses were projected onto the unit hemisphere. 2σ ellipses were also calculated using the data-covariance matrices from our measurements. To compare our technique with an established method, the SLM was deactivated, and ten 600-nm defocused images of Mol. 1 and Mol. 2 were acquired. Using template matching [6,9], independent orientation estimates were obtained. Since the simulated templates do not incorporate the minor optical aberrations that are present in the experimental system, results had lower precision, and may have systematic biases, thus highlighting the advantages of the quadrated pupil approach. Statistics are summarized in Table 1. Experimental precision compares favorably with similar methods [13–15].

We demonstrated our technique to be insensitive to minor defocus errors, an advantage over alternative image-matching schemes which must gauge depth to within a few nanometers in order to generate an appropriate set of templates. The objective lens was translated in 50-nm steps, with eleven frames of data recorded at each step (Mad City Labs, C-Focus). When the focal plane is within ± 150 nm of the layer of SMs, the orientation measurements are largely invariant [Fig. 2(g)], since there is little change in the major features of the images acquired using the quadrated pupil over this range [Fig. 2(h)].

Minor aberrations are mitigated, since orientation is inferred from intensity summed over coarse patches of pixels. As a consequence, our precision is generally slightly worse than what is predicted by the CRLB. However, if aberrations are present (a likely possibility when imaging thick biological samples), attempts at fine-scale image matching will introduce systematic errors, negating any gain in precision. To determine two-dimensional position, our scheme may be adapted by turning the SLM on and off, and taking two separate images. Furthermore, three-dimensional position may be measured by toggling between the quadrated phase mask and an astigmatic or double-helix [9] pattern.

This work was supported in part by the National Institute of General Medical Sciences grant R01GM085437. A. S. Backer acknowledges support from the National Defense Science and Engineering Graduate Fellowship. M. P. Backlund acknowledges support from a Robert and Marvel Kirby Stanford Graduate Fellowship. M. D. Lew acknowledges support from a National Science Foundation Graduate Research Fellowship and a 3Com Corporation Stanford Graduate Fellowship.

References

1. T. Ha, T. Enderle, D. S. Chemla, P. R. Selvin, and S. Weiss, Phys. Rev. Lett. **77**, 3979 (1996).
2. J. T. Fourkas, Opt. Lett. **26**, 211 (2001).
3. J. N. Forkey, M. E. Quinlan, and Y. E. Goldman, Biophys. J. **89**, 1261 (2005).
4. S. A. Rosenberg, M. E. Quinlan, J. N. Forkey, and Y. E. Goldman, Acc. Chem. Res. **38**, 583 (2005).
5. M. Böhmer and J. Enderlein, J. Opt. Soc. Am. B **20**, 554 (2003).
6. E. Toprak, J. Enderlein, S. Syed, S. A. McKinney, R. G. Petschek, T. Ha, Y. E. Goldman, and P. R. Selvin, Proc. Natl. Acad. Sci. USA **103**, 6495 (2006).
7. D. Axelrod, Methods Cell Biol. **30**, 333 (1989).
8. J. Engelhardt, J. Keller, P. Hoyer, M. Reuss, T. Staudt, and S. W. Hell, Nano Lett. **11**, 209 (2011).
9. M. P. Backlund, M. D. Lew, A. S. Backer, S. J. Sahl, G. Grover, A. Agrawal, R. Piestun, and W. E. Moerner, Proc. Natl. Acad. Sci. USA **109**, 19087 (2012).
10. E. H. Hellen and D. Axelrod, J. Opt. Soc. Am. B **4**, 337 (1987).
11. M. A. Lieb, J. M. Zavislan, and L. Novotny, J. Opt. Soc. Am. B **21**, 1210 (2004).
12. R. J. Ober, S. Ram, and E. S. Ward, Biophys. J. **86**, 1185 (2004).
13. F. Aguet, S. Geissbühler, I. Märki, T. Lasser, and M. Unser, Opt. Express **17**, 6829 (2009).
14. K. I. Mortensen, L. S. Churchman, J. A. Spudich, and H. Flyvbjerg, Nat. Methods **7**, 377 (2010).
15. S. Stallinga and B. Rieger, Opt. Express **20**, 6 (2012).